Sphinx Journal of Mathematical Sciences
1(1), 1–23, 2026
DOI: https://doi.org/10.64389/sjms.2026.011102
https://sphinxsp.org/journal/index.php/sjms/

Research article

Effect of Rotation on Wave Propagation in Micro-elongated Stochastic Thermo-elastic Media under the Refined Dual-Phase-Lag Model

Murat Yaylacı[1,*], Mohamed A. El-bassiouny [2]

[1,*] Department of Civil Engineering, Recep Tayyip Erdogan University, 53100, Rize, Türkiye, murat.yaylaci@erdogan.edu.tr

[2] Department of Mathematics and Computer Science, Faculty of Science, Alexandria University, Alexandria, Egypt; madel9406@gmail.com

* **Correspondence:** murat.yaylaci@erdogan.edu.tr

ARTICLE INFO

Keywords:
Micro-elongated
Refined Dual-Phase-Lag Model
Rotation
Stochastic system
Wiener Process

Mathematics Subject Classification:
74A15, 74A18, 93E03.

Important Dates:
Received: 1 December 2025
Revised: 26 December 2025
Accepted: 28 December 2025
Online: 1 January 2026

ABSTRACT

This work investigates the influence of rotational motion on wave propagation within a micro-elongated stochastic thermo-elastic medium. The governing relations describing elastic deformation, heat transport, and micro-elongation are formulated to accommodate finite thermal wave speeds and the additional degrees of freedom inherent in micro-structured materials. By applying an appropriate transform, the original coupled stochastic partial differential system is reduced to a set of stochastic ordinary differential equations that admit explicit analytical solutions. These solutions characterize the displacement field, micro-elongation behavior, stress components, and temperature distribution, enabling a comprehensive assessment of thermo-mechanical wave phenomena in a rotating environment. In addition, extensive numerical simulations are carried out to compare deterministic form and stochastic behaviors, with particular emphasis on how rotational effects and random thermal fluctuations modify the propagation characteristics.

1. Introduction

The Refined Dual-Phase-Lag (RDPL) model enhances modern heat conduction theory by providing a more comprehensive framework than the classical Dual-Phase-Lag (DPL) model [1, 2]. While the DPL model incorporates two separate phase delays associated with the temperature gradient and heat flux, respectively, it is typically inadequate to describe the complicated thermal delay mechanisms found in real materials subjected to rapid or high-intensity thermal loading. Ultra-fast thermal processes like advanced microelectronic cooling systems, and thermoelastic wave propagation show significant deviations from classical diffusion theory's predictions [3, 4]. To overcome these limitations, the RDPL model includes further refinements through higher-order phase-lag terms and strengthened constitutive relations, offering a more accurate depiction of materials' thermal response [5, 6]. These improvements allow the model to account for the limited speed of thermal wave propagation and the impact of material microstructure on energy transport processes [7]. Furthermore, the mathematical formulation and physical foundations of the RDPL model have been extensively developed. Owing to its improved accuracy, enhanced stability, and broader predictive capability, the RDPL model has emerged as an effective analytical tool for investigating thermoelastic phenomena in a wide range of contemporary engineering and scientific applications [8].

Micro-elongated thermoelastic materials are generalized continuum media that add internal degrees of freedom to the standard description of solid deformation [9, 10]. The micro-elongation theory adds a kinematic variable to account for local stretching or extension at the microstructural level, unlike traditional thermoelastic theories that only consider displacement fields and temperature variations [11, 12]. This micro-elongation method may involve fiber stretching, molecular chain extension, porous network deformation, or rearrangement of embedded microstructural constituents [13]. Microstructural components in such materials can deform independently of the body's displacement, which cannot be fully represented by classical continuum theories [14]. When thermal effects are included, the connection between the temperature field and the micro-elongation variable leads to additional stress contributions and heat transfer processes that are not included in traditional thermoelastic models [15]. The propagation of thermoelastic waves, stress field evolution, and temperature distribution in micro-elongated media exhibit distinct characteristics, including enhanced attenuation, dispersion, and relaxation effects that are strongly influenced by the internal microstructure of the material [16].

The impact of rotation on thermoelastic behavior is crucial for adequately understanding the mechanical and thermal reactions of materials with high angular velocities or rotational motion [17]. In rotating thermoelastic media, inertial effects from Coriolis and centrifugal forces must be integrated into the governing equations, as these forces considerably modify the dynamic properties of the system [18]. Rotational effects cause extra interaction between thermal and elastic fields, affecting wave propagation, stress, and temperature distributions within the material ([19]). Centrifugal force causes radial deformation, which can be stretching or compressing depending on the angular velocity and position within the medium, resulting in changes in the structure's equilibrium state and deformation patterns [20]. The Coriolis force causes directional dependence and frequency shifts in thermoelastic waves, which are not present in non-rotating situations [21]. Rotational contributions can significantly impact the speed, attenuation, and dispersion of thermoelastic disturbances [22, 23].

Stochastic thermo-elasticity is a sophisticated theoretical framework that enhances classical and generalized thermo-elastic models by integrating randomness into the mechanical and thermal behaviors of materials. In real-world engineering and physical systems, uncertainties arise from various sources, including fluctuations in material properties, imperfections in microstructure, environmental variability, external thermal disturbances, measurement noise, and random mechanical excitations. Conventional deterministic thermo-elastic theories don't sufficiently account for inherent uncertainties, frequently resulting in oversimplified forecasts that do not accurately represent the system's genuine behavior. The stochastic thermoelastic approach addresses this limitation by modeling the governing field equations such as the balance of momentum, energy equation, and constitutive relations with random parameters or stochastic processes, typically expressed through noise terms like Wiener processes [24] and white noise [25]. This probabilistic treatment allows the theory to describe not only the average response of the material but also the distribution, variability, and evolution of mechanical and thermal fields under uncertainty. As a result, quantities such as displacement, temperature, and stress become random fields whose statistical characteristics depend both on both parameters of the deterministic system and on stochastic perturbations for more details, see [26, 27]. Stochastic thermo-elastic models are essential for analyzing wave propagation, stability characteristics, and transient thermal responses in complex materials where randomness is significant, such as composite materials, microstructured solids, biological tissues, porous media, and systems subjected to variable thermal loads. The stochastic formulation offers insights into noise-induced attenuation, dispersion, resonance shifting, and reliability evaluation, which are crucial for designing structures that function in unpredictable situations.

This study examines the combined effect of rotational motion and stochastic disturbances on the thermo-elastic response of a micro-elongated half-space under the frameworks of the Loed-Shulman (L-S) Theory, the DPL model, and the RDPL model. The analysis begins with the formulation of the fundamental field equations governing mechanical motion, heat conduction, and micro-elongation. These equations are subsequently transformed into their non dimensional counterparts to facilitate analytical treatment. By employing the transform presented in Eq. (3.1), the original system of stochastic partial differential equations is converted into a more tractable system of stochastic ordinary differential equations. The boundary conditions specified at $z = 0$ are then imposed to determine the required constants and complete the solution procedure. Once analytical solutions are derived, they are utilized to carry out detailed numerical simulations and graphical evaluations aimed at assessing the impacts of rotation and stochastic excitation represented through white noise intensity on the distributions of displacement, temperature, stress, and micro-elongation within the medium.

2. Governing equations

This section describes the essential governing equations for two-dimensional micro-elongated stochastic thermo-elastic behavior within the frameworks of the L-S theory, DPL model, and RDPL model. The effect of rotational motion and stochastic disturbances on the system's thermomechanical response is studied. To aid analytical progress and simplify the problem's mathematical structure, the governing equations are further recast as non dimensional forms.

The equation of motion with rotation can be expressed in the following form [17]

$$\sigma_{ij,j} = \rho\left[u_{i,tt} + \{\mathbf{\Omega}\wedge(\mathbf{\Omega}\wedge\mathbf{u})\}_i + (2\mathbf{\Omega}\wedge\mathbf{u}_{,t})_i\right], \tag{2.1}$$

where

$$\sigma_{ij} = 2\mu\varepsilon_{ij} + (\lambda e - \gamma\Theta + \lambda_0\varphi)\,\delta_{ij}. \tag{2.2}$$

The equation of micro-elongated can be demonstrated by the following form [9]:

$$a_0\varphi_{,ii} + \gamma\Theta - \lambda_1\varphi - \lambda_0 u_{j,j} = \frac{\rho j^*\varphi_{,tt}}{2}. \tag{2.3}$$

The stochastic equation of energy under the RDPL model may be written in the following form [4, 24]:

$$0 \;=\; k\left(1 + \Sigma_{n=1}^{N}\frac{\tau_\theta^n}{n!}\frac{\partial^n}{\partial t^n}\right)\Theta_{,ii} - \gamma T_0\varphi_{,t}$$

$$-\left(1+\Sigma_{n=1}^{N}\frac{\tau_q^n}{n!}\frac{\partial^n}{\partial t^n}\right)\left[\gamma T_0\left(u_{,xt}+w_{,zt}\right)+\rho c_e\Theta_{,t}\right]+h\Theta_{,x}\alpha_t\frac{dW\left(t\right)}{dt},\tag{2.4}$$

when

1- $N=3$ and ($\tau_\theta<\tau_q\neq 0$, $k\neq 0$) is RDPL model,

2- $N=1$ and ($\tau_\theta<\tau_q\neq 0$, $k\neq 0$) is DPL model,

3- $N=1$ and ($\tau_\theta=0$, $\tau_q\neq 0$, $k\neq 0$) is L-S theory,

where, $W(t)$ represents the Wiener process, while $\frac{dW(t)}{dt}$ is the white noise term, and h denotes the intensity of the white noise acting on the system.

The Wiener process is distinguished by several essential statistical features, which are given below [30, 31]:

i: For $r<t$, $W(t)-W(r)$ has independent increments.

ii: For $0\leq t$, $W(t)$ has continuous trajectories.

iii: $W(t)-W(r)$ has a normal distribution with variance $=t-r$ and mean $=0$.

From Eq. (2.2) in Eq. (2.1) with the aid of the displacement vector $\mathbf{u}\left(x,z,t\right)=u\left(u,0,w\right)$, we see

$$\mu\nabla^2 u+\left(\lambda+\mu\right)e_{,x}-\gamma\Theta_{,x}+\lambda_0\varphi_{,x}=\rho\left[u_{,tt}-\Omega^2 u+2\Omega w_{,t}\right],\tag{2.5}$$

$$\mu\nabla^2 w+\left(\lambda+\mu\right)e_{,z}-\gamma\Theta_{,z}+\lambda_0\varphi_{,z}=\rho\left[w_{,tt}-\Omega^2 w-2\Omega u_{,t}\right].\tag{2.6}$$

Employing the displacement vector $\mathbf{u}\left(x,z,t\right)=u\left(u,0,w\right)$ in Eq. (2.3), we infer

$$a_0\varphi_{,ii}+\gamma\Theta-\lambda_1\varphi-\lambda_0\left(u_{,x}+w_{,z}\right)=\frac{\rho j^*\varphi_{,tt}}{2}.\tag{2.7}$$

In this analysis, we employ the following nondimensional variables to streamline the governing equations

$$\begin{aligned}(u,\ v)&=\frac{T_0\gamma}{\rho c_1\omega^*}\left(\bar{u},\ \bar{v}\right),\ \left(x,z\right)=\frac{c_1}{\omega^*}\left(\bar{x},\ \bar{z}\right),\ \Theta=T_0\bar{\Theta},\ \left(t,\ \tau_\theta,\ \tau_q\right)=\frac{\left(\bar{t},\ \bar{\tau}_\theta,\ \bar{\tau}_q\right)}{\omega^*},\ \sigma_{ij}=\gamma T_0\bar{\sigma}_{ij},\\ \varphi&=\frac{\gamma T_0}{\lambda_0}\bar{\varphi},\ \Omega=\omega^*\bar{\Omega},\ k\omega^*=\rho c_1^2 c_e,\ \rho c_1^2=\lambda+\mu.\end{aligned}\tag{2.8}$$

Utilizing Eq. (2.8) in Eq. (2.5), one uncovers

$$\left(\varsigma_1\nabla^2-\frac{\partial^2}{\partial t^2}+\varsigma_2\frac{\partial^2}{\partial x^2}+\Omega^2\right)u+\left(\varsigma_2\frac{\partial^2}{\partial x\partial z}-2\Omega\frac{\partial}{\partial t}\right)w-\frac{\partial\Theta}{\partial x}+\frac{\partial\varphi}{\partial x}=0,\tag{2.9}$$

Using Eq. (2.8) in Eq. (2.6), we discover

$$\left(\varsigma_2\frac{\partial^2}{\partial x\partial z}+2\Omega\frac{\partial}{\partial t}\right)u+\left(\varsigma_1\nabla^2-\frac{\partial^2}{\partial t^2}+\varsigma_2\frac{\partial^2}{\partial z^2}+\Omega^2\right)w-\frac{\partial\Theta}{\partial z}+\frac{\partial\varphi}{\partial z}=0,\tag{2.10}$$

Employing Eq. (2.8) in Eq. (2.7), one infers

$$\varsigma_5\frac{\partial u}{\partial x}+\varsigma_5\frac{\partial w}{\partial z}-\varsigma_3\Theta-\left(\nabla^2-\varsigma_4-\varsigma_6\frac{\partial^2}{\partial t^2}\right)\varphi=0,\tag{2.11}$$

From Eq. (2.8) in Eq. (2.4), we acquire

$$\varsigma_8(1+\tau_2)\frac{\partial^2 u}{\partial x\partial t}+\varsigma_8(1+\tau_2)\frac{\partial^2 w}{\partial z\partial t}-\left(\nabla^2+\tau_1\nabla^2-\varsigma_7\frac{\partial}{\partial t}-\tau_2\varsigma_7\frac{\partial}{\partial t}\right)\Theta+\frac{\alpha_t hc_1}{kw^*}\frac{\partial\Theta}{\partial x}\frac{dW(t)}{dt}+\varsigma_9\frac{\partial\varphi}{\partial t}=0, \quad (2.12)$$

where, $\varsigma_1=\frac{\mu}{c_1^2\rho}$, $\varsigma_2=\frac{\mu+\lambda}{c_1^2\rho}$, $\varsigma_3=\frac{\lambda_0\gamma c_1^2}{\gamma a_0\omega^{*2}}$, $\varsigma_4=\frac{c_1^2\lambda_1}{a_0\omega^{*2}}$, $\varsigma_5=\frac{\lambda_0^2}{a_0\rho\omega^{*2}}$, $\varsigma_6=\frac{\rho j^* c_1^2}{2a_0}$,
$\varsigma_7=\frac{\rho c_e c_1^2}{k\omega^*}$, $\varsigma_8=\frac{\gamma^2 T_0}{k\omega^*\rho}$, $\varsigma_9=\frac{\gamma^2 T_0 c_1^2}{k\omega^*\lambda_0}$, $\tau_1=\Sigma_{n=1}^{N}\frac{\tau_\theta^n}{n!}\frac{\partial^n}{\partial t^n}$, and $\tau_2=\Sigma_{n=1}^{N}\frac{\tau_q^n}{n!}\frac{\partial^n}{\partial t^n}$.

Employing Eq. (2.8) in Eq. (2.2), we acquire

$$\sigma_{xx}=\frac{\partial u}{\partial x}+\varsigma_{10}\frac{\partial w}{\partial z}-\Theta+\varphi, \quad (2.13)$$

$$\sigma_{zz}=\varsigma_{10}\frac{\partial u}{\partial x}+\frac{\partial w}{\partial z}-\Theta+\varphi, \quad (2.14)$$

$$\sigma_{zx}=\sigma_{xz}=\varsigma_1\frac{\partial u}{\partial z}+\varsigma_1\frac{\partial w}{\partial x}. \quad (2.15)$$

where, $\varsigma_{10}=\frac{\lambda_0^2}{a_0\rho\omega^{*2}}$.

The displacement potentials $\eta(x,\ z,\ t)$ and $\zeta(x,\ z,\ t)$ that relate to displacement components have been introduced,we realize

$$u=\eta_{,x}+\zeta_{,z},\qquad w=\eta_{,z}-\zeta_{,x}. \quad (2.16)$$

From Eq. (2.16) in Eqs. (2.9), (2.10), (2.11), and (2.12), we realize

$$\left[(\varsigma_1+\varsigma_2)\nabla^2+\Omega^2-\frac{\partial^2}{\partial t^2}\right]\eta+2\Omega\zeta_{,t}-\Theta+\varphi=0, \quad (2.17)$$

$$2\Omega\eta_{,t}-\left[\varsigma_1\nabla^2+\Omega^2-\frac{\partial^2}{\partial t^2}\right]\zeta=0, \quad (2.18)$$

$$\varsigma_5\nabla^2\eta-\varsigma_3\Theta-\left(\nabla^2-\varsigma_4-\varsigma_6\frac{\partial^2}{\partial t^2}\right)\varphi=0, \quad (2.19)$$

$$\varsigma_8(1+\tau_2)\nabla^2\left(\frac{\partial\eta}{\partial t}\right)-\left(\nabla^2+\tau_1\nabla^2-\varsigma_7\frac{\partial}{\partial t}-\tau_2\varsigma_7\frac{\partial}{\partial t}\right)\Theta+\frac{\alpha_t hc_1}{kw^*}\frac{\partial\Theta}{\partial x}\frac{dW(t)}{dt}+\varsigma_9\frac{\partial\varphi}{\partial t}=0. \quad (2.20)$$

3. Main Results

In this section, we use the following wave transformation to build every potential solutions:

$$\left[u,\ w,\ \Theta,\ \varphi,\ \eta,\ \zeta,\ \sigma_{ij}\right](x,\ z,\ t)=\left[\tilde{u},\ \tilde{w},\ \tilde{\Theta},\ \tilde{\varphi},\ \tilde{\eta},\ \tilde{\zeta},\ \tilde{\sigma}_{ij}\right](z)\,e^{i\left(bx-\omega t+hW(t)-h^2t\right)}. \quad (3.1)$$

where, ω is the wave number and b is the frequency

Inserting Eq. (3.1) into Eqs. (2.17), (2.18), (2.19), and (2.20), we realize

$$\left(\xi_1 D^2+\xi_2\right)\tilde{\eta}+\xi_3\tilde{\zeta}-\tilde{\Theta}+\tilde{\varphi}=0, \quad (3.2)$$

$$\xi_3\tilde{\eta}-\left[\varsigma_1 D^2+\xi_4\right]\tilde{\zeta}=0, \quad (3.3)$$

$$\left[\varsigma_5 D^2-\xi_5\right]\tilde{\eta}-\varsigma_3\tilde{\Theta}-\left(D^2+\xi_6\right)\tilde{\varphi}=0, \tag{3.4}$$

$$\left[\xi_7 D^2-\xi_8\right]\tilde{\eta}-\left(\xi_9 D^2-\xi_{10}\right)\tilde{\Theta}+\xi_{11}\tilde{\varphi}=0, \tag{3.5}$$

where, $\xi_1=\varsigma_1+\varsigma_2$, $\xi_2=\left(\omega+h^2-h\frac{dW(t)}{dt}\right)^2+\Omega^2-b^2\xi_1$, $\xi_3=-2i\Omega\left(\omega+h^2-h\frac{dW(t)}{dt}\right)$,
$\xi_4=\left(\omega+h^2-h\frac{dW(t)}{dt}\right)^2+\Omega^2-\varsigma_1 b^2$, $\xi_5=-b^2\varsigma_5$,
$\xi_6=\varsigma_6\left(\omega+h^2-h\frac{dW(t)}{dt}\right)^2-\varsigma_4-b^2$, $\xi_7=-i\varsigma_8\left(1+\tau_2\right)\left(\omega+h^2-h\frac{dW(t)}{dt}\right)$,
$\xi_8=\xi_7 b^2$, $\xi_9=\left(1+\tau_1\right)$, $\xi_{10}=\xi_9 b^2+i\varsigma_7\left(1+\tau_2\right)\left(-\omega-h^2+h\frac{dW(t)}{dt}\right)-ib\frac{\alpha_t hc_1}{kw^*}\frac{dW(t)}{dt}$
$\xi_{11}=-i\varsigma_9\left(\omega+h^2-h\frac{dW(t)}{dt}\right)$.
It is observed that the cases

1. $\tau_1=\left(\omega+h^2-h\frac{dW(t)}{dt}\right)\tau_\theta\left[-i-\left(\omega+h^2-h\frac{dW(t)}{dt}\right)\frac{\tau_\theta}{2}+i\left(\omega+h^2-h\frac{dW(t)}{dt}\right)^2\frac{\tau_\theta^2}{6}\right]$ and $\tau_2=\left(\omega+h^2-h\frac{dW(t)}{dt}\right)\tau_q\left[-i-\left(\omega+h^2-h\frac{dW(t)}{dt}\right)\frac{\tau_q}{2}+i\left(\omega+h^2-h\frac{dW(t)}{dt}\right)^2\frac{\tau_q^2}{6}\right]$ correspond to the RDPL model
2. $\tau_1=-i\left(\omega+h^2-h\frac{dW(t)}{dt}\right)\tau_\theta$ and $\tau_2=-i\left(\omega+h^2-h\frac{dW(t)}{dt}\right)\tau_q$ correspond to the DPL model
3. $\tau_1=0$ and $\tau_2=-i\left(\omega+h^2-h\frac{dW(t)}{dt}\right)\tau_q$ correspond to the L-S theory

Equations (3.2), (3.4), and (3.5) yield a nontrivial solution when the determinant of the coefficient matrix associated with the physical quantities equals zero. Using the MATLAB program, we acquire

$$\left(D^8-B_1D^6+B_2D^4-B_3D^2+B_4\right)\{\tilde{\eta}(z),\tilde{\zeta}(z),\ \tilde{\Theta}(z),\ \tilde{\varphi}(z)\}=0, \tag{3.6}$$

where, $B_1=\frac{-1}{\xi_1\xi_9\varsigma_1}\{-\xi_7\varsigma_1+\xi_9\varsigma_1\varsigma_5+\xi_1\xi_4\xi_9-\xi_1\xi_{10}\varsigma_1+\xi_2\xi_9\varsigma_1+\xi_1\xi_6\xi_9\varsigma_1\}$,
$B_2=\frac{1}{\xi_1\xi_9\varsigma_1}\{\xi_4\xi_7+\xi_3^2\xi_9-\xi_7\varsigma_1\varsigma_3-\xi_{10}\varsigma_1\varsigma_5-\xi_{11}\varsigma_1\varsigma_5-\xi_1\xi_4\xi_{10}+\xi_2\xi_4\xi_9-\xi_2\xi_{10}\varsigma_1-\xi_6\xi_7\varsigma_1$
$-\xi_5\xi_9\varsigma_1+\xi_4\xi_9\varsigma_5+\xi_1\xi_4\xi_6\xi_9-\xi_1\xi_6\xi_{10}\varsigma_1+\xi_2\xi_6\xi_9\varsigma_1+\xi_1\xi_{11}\varsigma_1\varsigma_3+\xi_8\varsigma_1\}$,
$B_3=\frac{-1}{\xi_1\xi_9\varsigma_1}\{\xi_4\xi_8+\xi_3^2\xi_6\xi_9-\xi_2\xi_4\xi_{10}-\xi_4\xi_6\xi_7-\xi_4\xi_5\xi_9-\xi_4\xi_7\varsigma_3+\xi_6\xi_8\varsigma_1+\xi_5\xi_{10}\varsigma_1+\xi_5\xi_{11}\varsigma_1$
$-\xi_4\xi_{10}\varsigma_5-\xi_4\xi_{11}\varsigma_5-\xi_1\xi_4\xi_6\xi_{10}+\xi_2\xi_4\xi_6\xi_9+\xi_1\xi_4\xi_{11}\varsigma_3-\xi_2\xi_6\xi_{10}\varsigma_1+\xi_2\xi_{11}\varsigma_1\varsigma_3-\xi_3^2\xi_{10}+\xi_8\varsigma_1\varsigma_3\}$,
$B_4=\frac{1}{\xi_1\xi_9\varsigma_1}\{\xi_4\xi_6\xi_8+\xi_4\xi_5\xi_{10}+\xi_4\xi_5\xi_{11}+\xi_4\xi_8\varsigma_3-\xi_3^2\xi_6\xi_{10}+\xi_3^2\xi_{11}\varsigma_3-\xi_2\xi_4\xi_6\xi_{10}+\xi_2\xi_4\xi_{11}\varsigma_3\}$.
This equation can be expressed as

$$\left(D^2-s_1\right)\left(D^2-s_2\right)\left(D^2-s_3\right)\left(D^2-s_4\right)\{\tilde{\eta}(z),\ \tilde{\zeta}(z),\ \tilde{\Theta}(z),\ \tilde{\varphi}(z)\}=0, \tag{3.7}$$

where, s_1, s_2, s_3 and s_4 are roots

The general solution of Eq. (3.7) bound as $z\to\infty$ can be written as

$$\tilde{\eta}(z)=\Sigma_{m=1}^4 G_m e^{-s_m z}, \tag{3.8}$$

$$\tilde{\zeta}(z)=\Sigma_{m=1}^4 \vartheta_{1m}G_m e^{-s_m z} \tag{3.9}$$

$$\tilde{\Theta}(z)=\Sigma_{m=1}^4 \vartheta_{2m}G_m e^{-s_m z}, \tag{3.10}$$

$$\tilde{\varphi}(z)=\Sigma_{m=1}^4 \vartheta_{3m}G_m e^{-s_m z}. \tag{3.11}$$

where, $\vartheta_{1m}=\frac{\xi_3}{\varsigma_1 s_m^2+\xi_4}$, $\vartheta_{2m}=\frac{\xi_7 s_m^4+(\xi_6\xi_7-\xi_8)s_m^2-\xi_5\xi_{11}-\xi_6\xi_8}{\xi_9 s_m^4+(\xi_6\xi_9-\xi_{10})s_m^2-\xi_6\xi_{10}-\varsigma_3\xi_{11}}$, and $\vartheta_{3m}=-\left(\xi_1 s_m^2+\xi_2\right)-\xi_3\ \vartheta_{1m}+\ \vartheta_{2m}$.

Using Eq. (3.1) in Eq. (2.16), then employing Eqs. (3.8) and (3.9), one sees

$$\tilde{u} = -\Sigma_{m=1}^{4}\left(s_m\vartheta_{1m} + ib\right)G_m e^{-s_m z}, \tag{3.12}$$

$$\tilde{w} = \Sigma_{m=1}^{4}\left(ib\vartheta_{1m} - s_m\right)G_m e^{-s_m z}. \tag{3.13}$$

Utilizing Eq. (3.1) into Eqs. (2.13), (2.14), and (2.15), then using Eqs. (3.10), (3.11), (3.12) and (3.13), we infer

$$\tilde{\sigma}_{xx} = \Sigma_{m=1}^{4}\vartheta_{4m}G_m e^{-s_m z}, \tag{3.14}$$

$$\tilde{\sigma}_{zz} = \Sigma_{m=1}^{4}\vartheta_{5m}G_m e^{-s_m z}, \tag{3.15}$$

$$\tilde{\sigma}_{xz} = \tilde{\sigma}_{zx} = \Sigma_{m=1}^{4}\vartheta_{6m}G_m e^{-s_m z}, \tag{3.16}$$

where, $\vartheta_{4m} = ib\left(1-\varsigma_{10}\right)s_m\vartheta_{1m} + \varsigma_{10}s_m^2 - b^2 - \vartheta_{2m} + \vartheta_{3m}$,
$\vartheta_{5m} = ib\left(\varsigma_{10}-1\right)s_m\vartheta_{1m} + s_m^2 - \varsigma_{10}b^2 - \vartheta_{2m} + \vartheta_{3m}$, $\vartheta_{6m} = \varsigma_1\left(s_m^2 + b^2\right)\vartheta_{1m} + 2ib\varsigma_1 s_m$.
To find the constants (G_1, G_2, G_3, and G_4), we have applied the boundary conditions for the problem at $z = 0$ as follows:

$$\sigma_{zz} = f_1 e^{i\left(bx-\omega t+hW(t)-h^2t\right)},\ \sigma_{xz} = 0,\ \Theta = f_2 e^{i\left(bx-\omega t+hW(t)-h^2t\right)},\ \frac{\partial\varphi}{\partial z} = 0, \tag{3.17}$$

where f_1 and f_2 are constants.

Substituting the assumed functional forms of the variables into the boundary conditions given in (3.17), yields a set of relations that the system parameters must satisfy. This procedure leads to a system of four linear equations. To evaluate the unknown constants (G_1, G_2, G_3, and G_4) the system is solved using the inverse matrix technique as shown below:

$$\begin{bmatrix} G_1 \\ G_2 \\ G_3 \\ G_4 \end{bmatrix} = \begin{bmatrix} \vartheta_{51} & \vartheta_{52} & \vartheta_{53} & \vartheta_{54} \\ \vartheta_{61} & \vartheta_{62} & \vartheta_{63} & \vartheta_{64} \\ \vartheta_{21} & \vartheta_{22} & \vartheta_{23} & \vartheta_{24} \\ -s_1\vartheta_{31} & -s_2\vartheta_{32} & -s_3\vartheta_{33} & -s_4\vartheta_{34} \end{bmatrix}^{-1} \begin{bmatrix} f_1 \\ 0 \\ f_2 \\ 0 \end{bmatrix} \tag{3.18}$$

4. Numerical discussions and results

This section presents a series of graphical representations depicting the obtained solutions in a two-dimensional framework. These visual illustrations play a crucial role in revealing the evolution of the key field variables, thereby enhancing the physical interpretation of the results and clarifying the qualitative patterns exhibited by the system. For the numerical analysis, an aluminum–epoxy composite is chosen as the representative thermo-elastic material due to its well-established thermal and mechanical properties, which render it highly suitable for examining coupled thermo-elastic responses. the numerical values used in the computations are summarized in the following [9]:

$$j^* = 0.196\times10^{-4}\ \mathrm{m}^2,\qquad \lambda = 7.59\times10^{10}\ \frac{\mathrm{N}}{\mathrm{m}^2},\qquad \rho = 2190\ \frac{\mathrm{kg}}{\mathrm{m}^3},$$

$$\mu = 1.89\times10^{10}\ \frac{\mathrm{N}}{\mathrm{m}^2},\qquad \gamma = 0.50\times10^{5}\ \frac{\mathrm{N}}{\mathrm{m}^2.\mathrm{K}},\qquad \lambda_0 = 0.37\times10^{10}\ \frac{\mathrm{N}}{\mathrm{m}^2},$$

$$a_0 = 0.61\times10^{-10},\quad c_e = 966\,\frac{\mathrm{J}}{\mathrm{kg.K}},\quad k = 252\,\frac{\mathrm{J}}{\mathrm{m.s.K}},\quad T_0 = 293^\circ\ \mathrm{K},$$
$$\lambda_1 = 0.37\times10^{10}\,\frac{\mathrm{N}}{\mathrm{m}^2},\quad \tau_\theta = 0.6\ \mathrm{s},\quad \tau_q = 0.9\ \mathrm{s}\quad f_1 = 15,\quad f_2 = 10.$$

In this paper, the numerical evaluations of all physical quantities are performed at the non-dimensional time $t = 1$ across the spatial domain $0 \le z \le 5$ and along the surface $x = 1.5$. The numerical technique employed in this work is used to examine and describe the behavior and variations of the physical quantities u, w, Θ, φ, σ_{xx}, σ_{zz}, and σ_{xz}. Figures (1, 2, 3, 4, 5, 6, and 7) show a complete comparison of deterministic and stochastic field responses in the RDPL model, demonstrating how stochastic excitation alters wave properties in a rotating ($\Omega = 2$) micro-elongated thermo-elastic medium. Figures (1 and 2,) depict the horizontal and vertical displacement components. When subjected to stochastic stimulation, both displacement fields show substantial variations and amplitude modulation in comparison to the deterministic scenario. This suggests that random thermal disturbances have a considerable influence on mechanical motion, resulting in amplified oscillations and greater sensitivity to microstructural changes. The rotating effect amplifies these aberrations, making displacement waves more dispersed and energetically unstable. Figure (3) depicts temperature distribution, reveals that stochastic heating causes greater fluctuation and irregular oscillations, indicating the direct influence of stochastic on the energy equation. Figure (4) illustrates how the micro-elongation field is influenced by stochastic disturbances. The stochastic response exhibits noticeable fluctuations and modified attenuation patterns compared with the deterministic case, highlighting the heightened sensitivity of micro-elongation to random effects. This behavior arises because the micro-elongation variable is strongly coupled with both the displacement and temperature fields, causing noise-induced irregularities to be amplified throughout the system. Figures (5, 6, and 7,) illustrate the stress components σ_{xx}, σ_{zz}, and σ_{xz} with the distance z. The stochastic stresses display greater damping, faster decay rates, and irregular response patterns compared with the deterministic profiles. This behavior emphasizes the sensitivity of the stress field to random excitations, especially in rotating environments where Coriolis and centrifugal forces further influence stability. Figures (8, 9, 10, 11, 12, 13, and 14) compare deterministic and stochastic field responses in the DPL model, demonstrating how stochastic excitation affects wave characteristics in a rotating ($\Omega = 2$) micro-elongated thermo-elastic medium. Figures (8) and (9) reveal that displacement fields under the DPL model experience amplified oscillations and higher wave distortion when exposed to stochastic, suggesting that the DPL model provides less damping and weaker control over random disturbances. Figure (10) illustrates that the temperature evolution under the DPL model is considerably influenced by stochasticity, with higher fluctuations and irregular peaks than the RDPL model. Figure (11) depicts the relation between micro-elongation and distance z. It is clear that the values of micro-elongation have sharper deviations and less smooth decay in the stochastic case, indicating that the DPL model does not suppress noise-induced microstructural variations as effectively as the RDPL framework. Figures (12, 13, and 14) depict the three stress components with distance z. The values of the three stress components exhibit more prominent oscillating patterns when subjected to stochastic forcing. Stress waves propagate with less damping and greater instability than those shown in figures (5, 6, and 7). The lower stability suggests that the DPL model is more vulnerable to noise and rotational effects. Figures (15, 16, 17, 18, 19, 20, and 21) compare deterministic and stochastic responses in the L-S theory, revealing how stochastic excitation affects wave characteristics in a rotating ($\Omega = 2$) micro-elongated thermo-elastic medium. Figures (15 and 16) display the displacement components under stochastic and deterministic conditions. In the stochastic scenario, the displacement components significantly amplify wave oscillations.

The absence of DPL mechanisms prevents the L-S theory from completely capturing finite thermal wave speed in noisy environments, resulting in very varied displacement. Figure (17) shows the temperature under stochastic and deterministic conditions. it is obvious that the temperature values have greater fluctuations than DPL model and RDPL model, confirming that the L-S theory provides only limited control over random thermal. Figure (18) depicts the micro-elongation with distance z. The values of micro-elongation reveal significant irregularity and more pronounced noise amplification. This demonstrates the strong relationship between microstructural deformation, rotation, and stochastic thermal excitation. Figures (19, 20, and 21) illustrate the stress components against the distance z. The values of the stress components demonstrate the greatest divergence between deterministic and stochastic responses among all three models. Stress waves under the L-S theory have weaker damping, more oscillatory behavior, and sharper gradients.

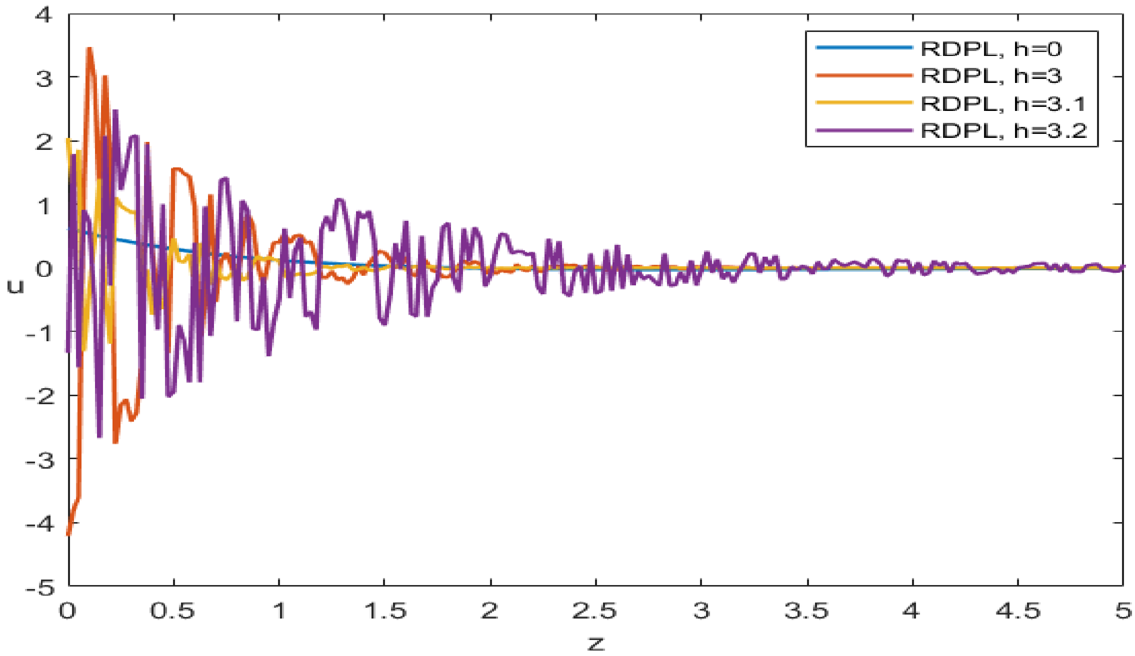

Figure 1. The horizontal displacement distributions for the RDPL model

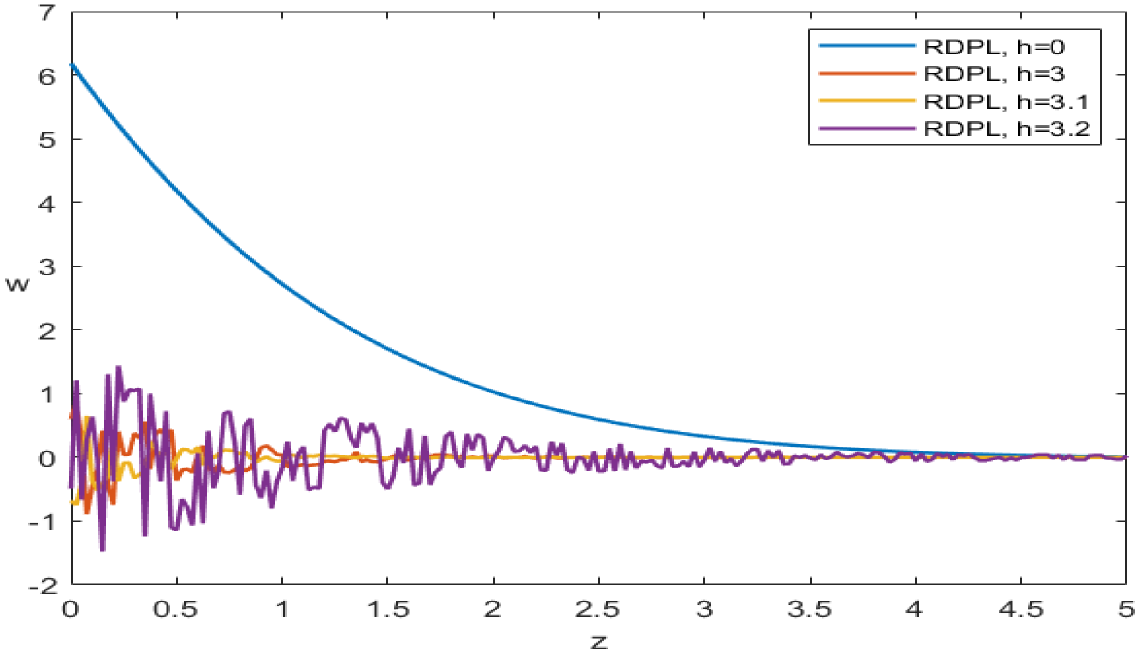

Figure 2. The vertical displacement distributions for the RDPL model

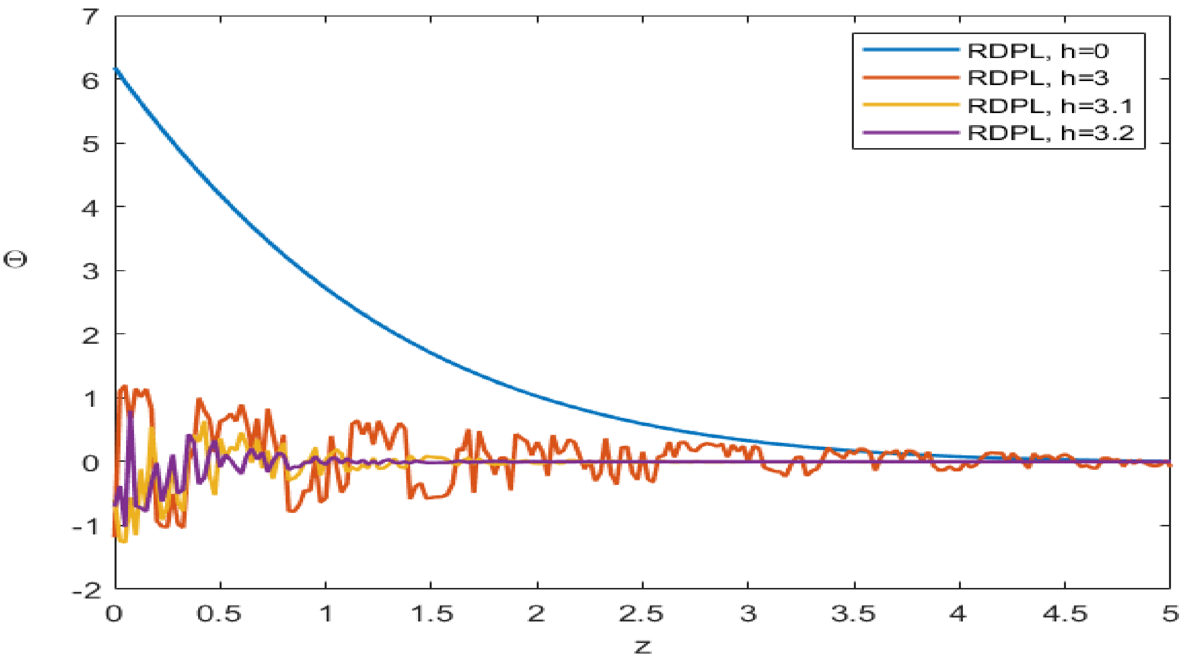

Figure 3. The temperature distributions for the RDPL model

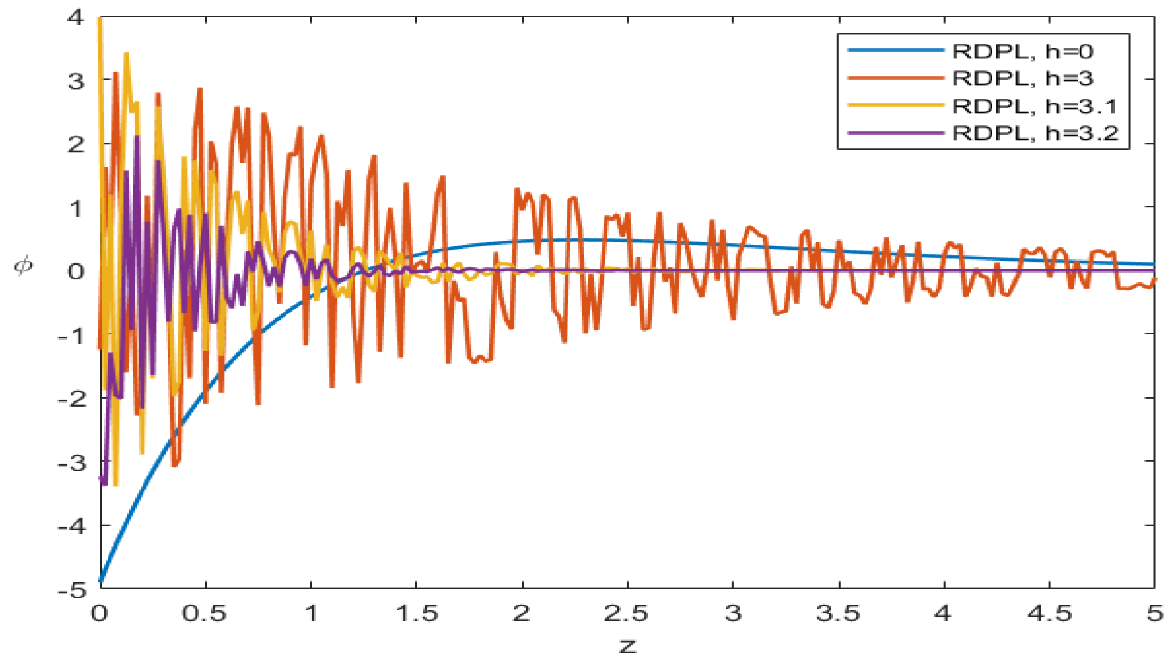

Figure 4. The micro-elongated distributions for the RDPL model

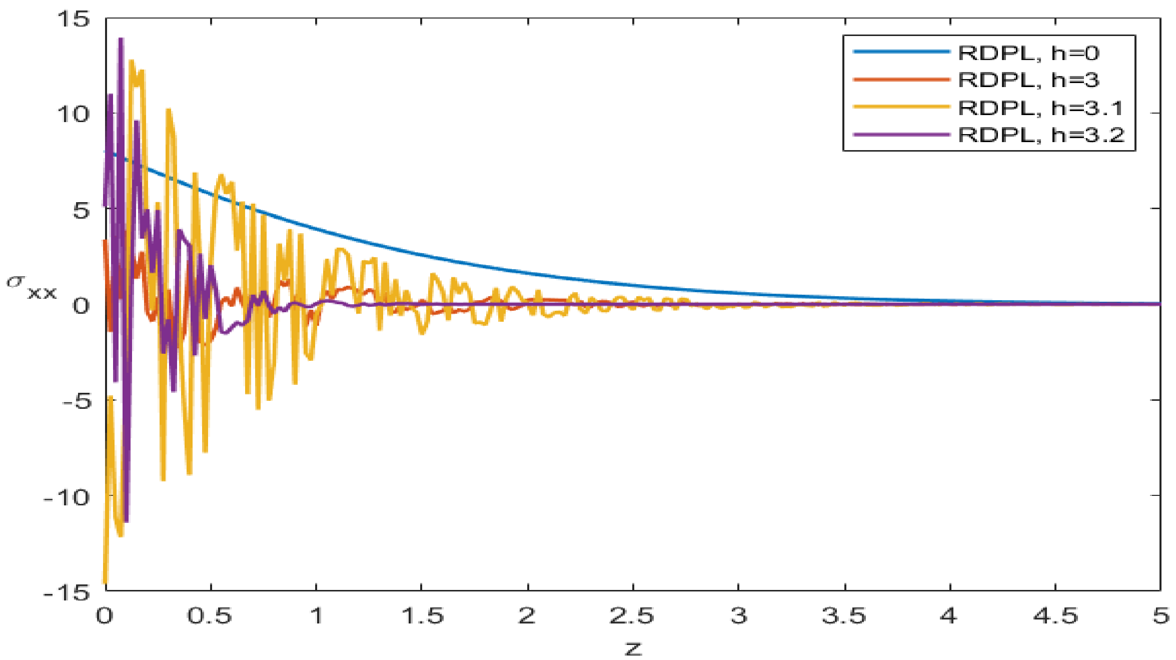

Figure 5. The stress tensor (σ_{xx}) distributions for the RDPL model

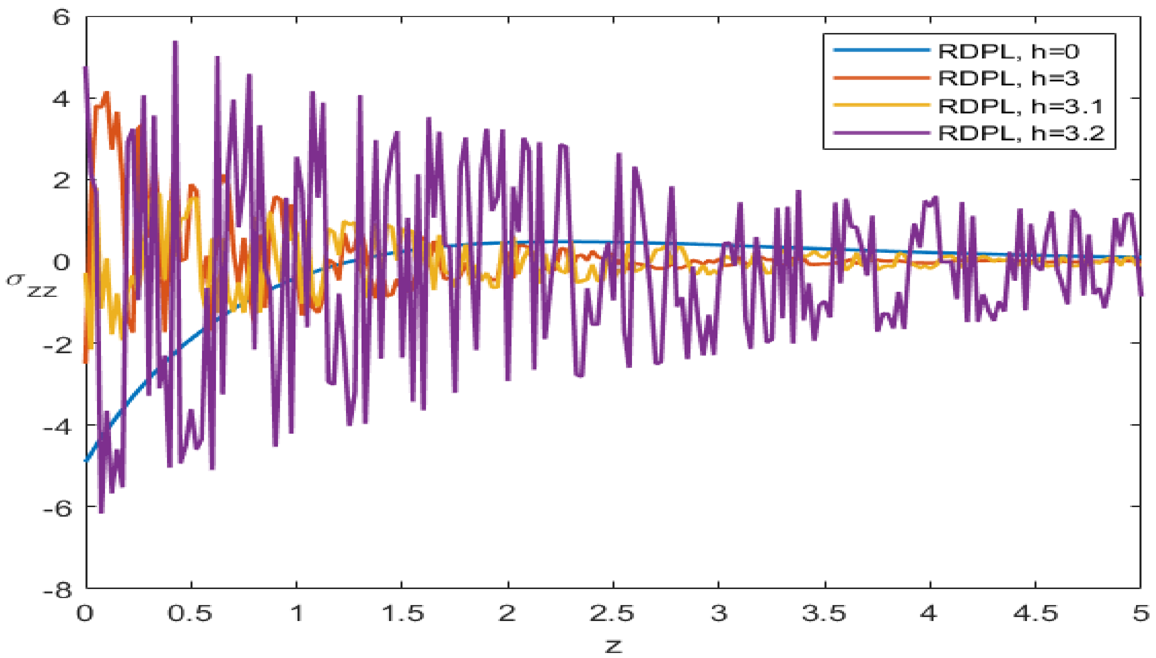

Figure 6. The stress tensor (σ_{zz}) distributions for the RDPL model

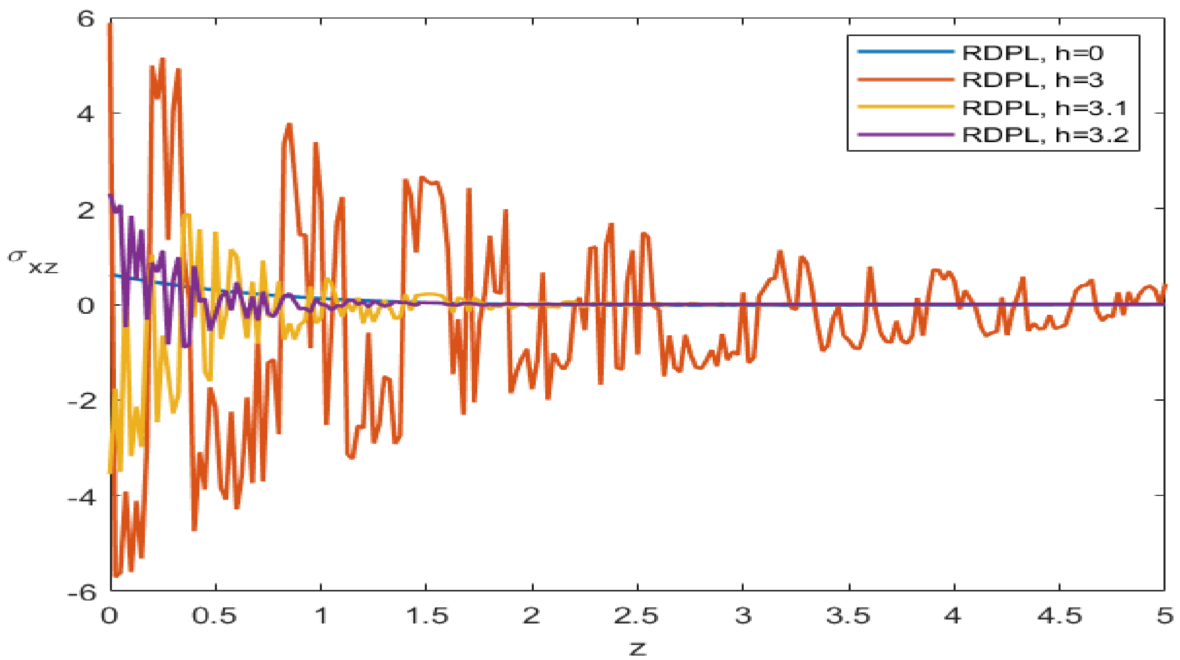

Figure 7. The stress tensor (σ_{xz}) distributions for the RDPL model

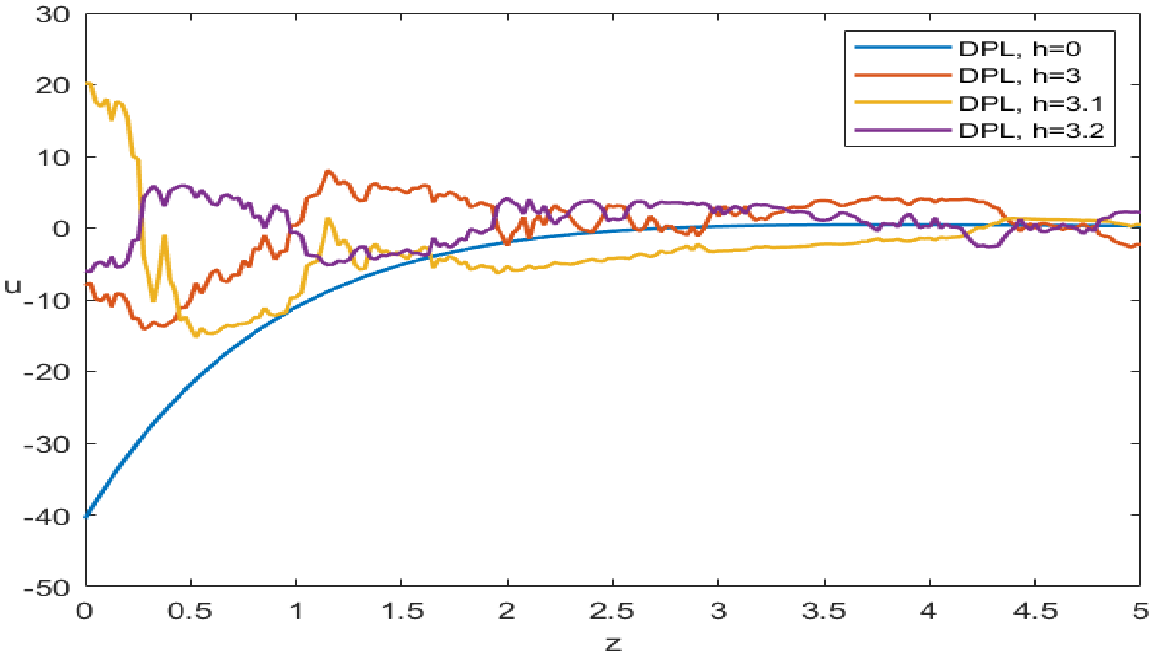

Figure 8. The horizontal displacement distributions for the DPL model

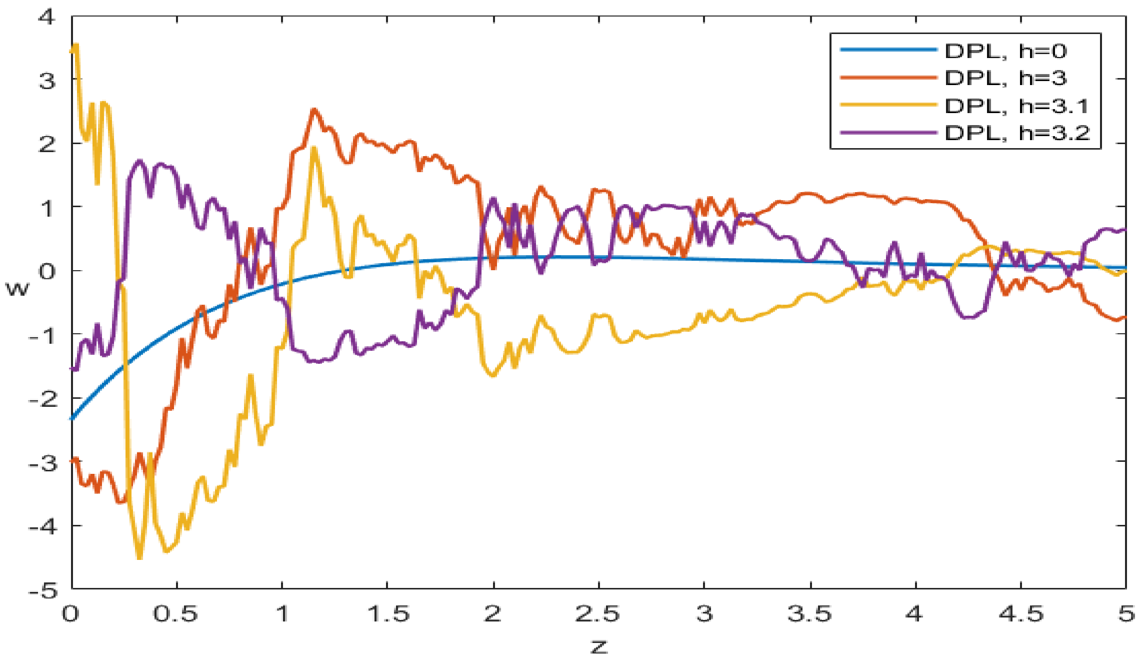

Figure 9. The vertical displacement distributions for the DPL model

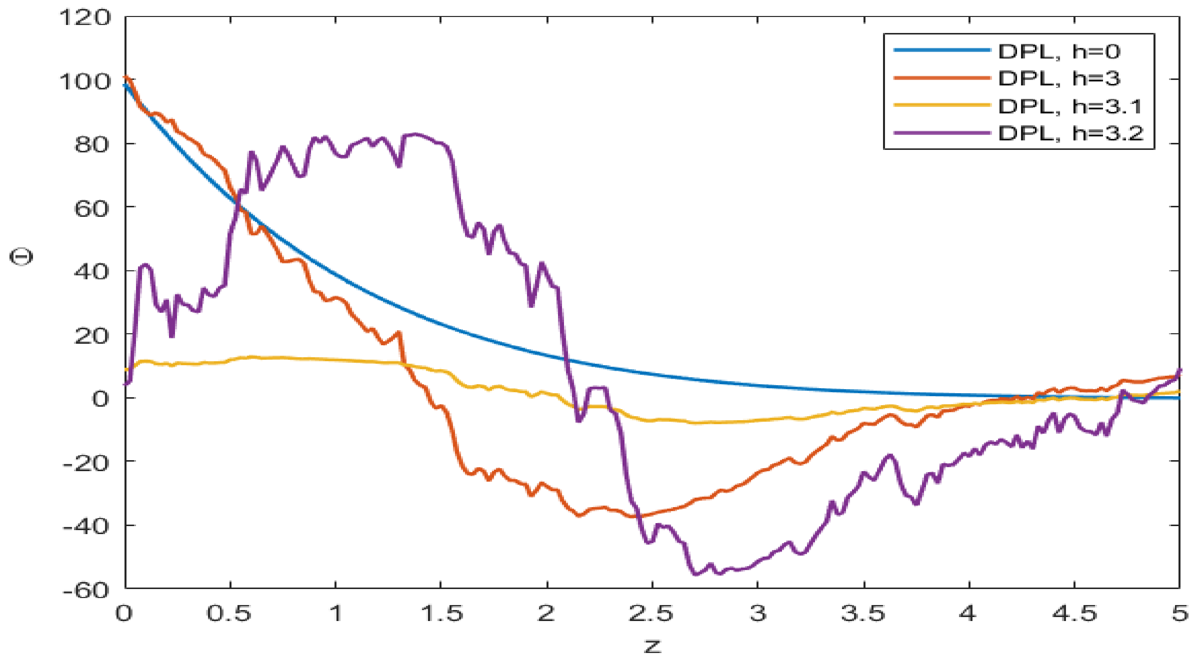

Figure 10. The temperature distributions for the DPL model

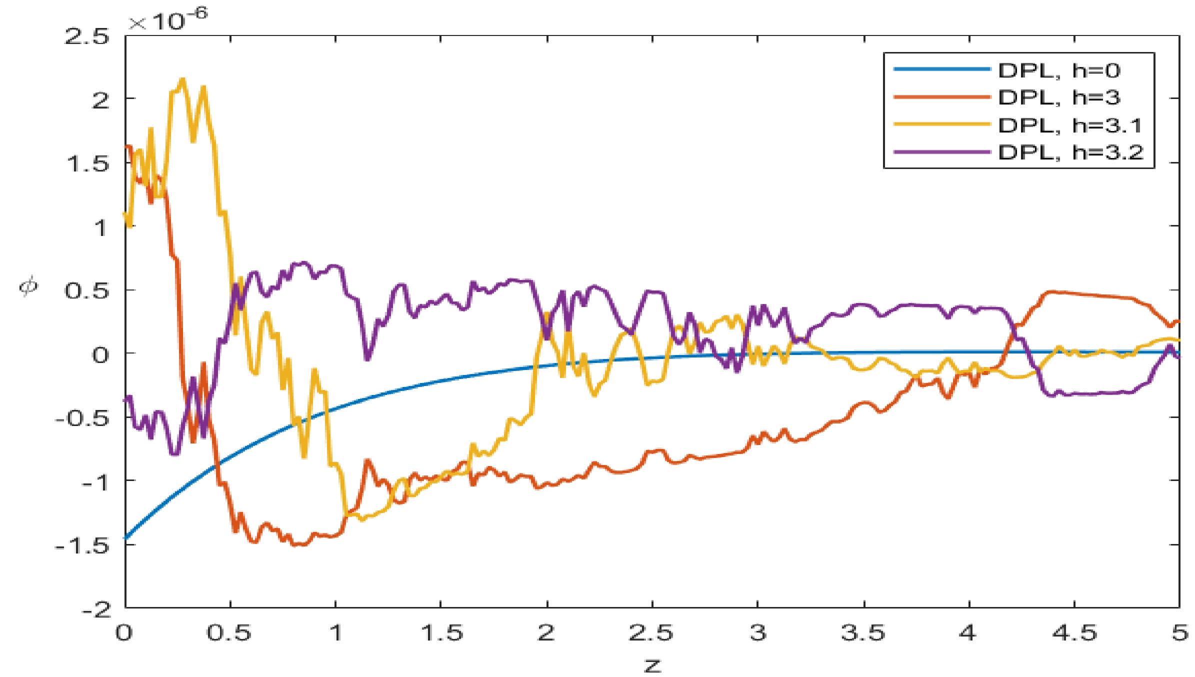

Figure 11. The micro-elongated distributions for the DPL model

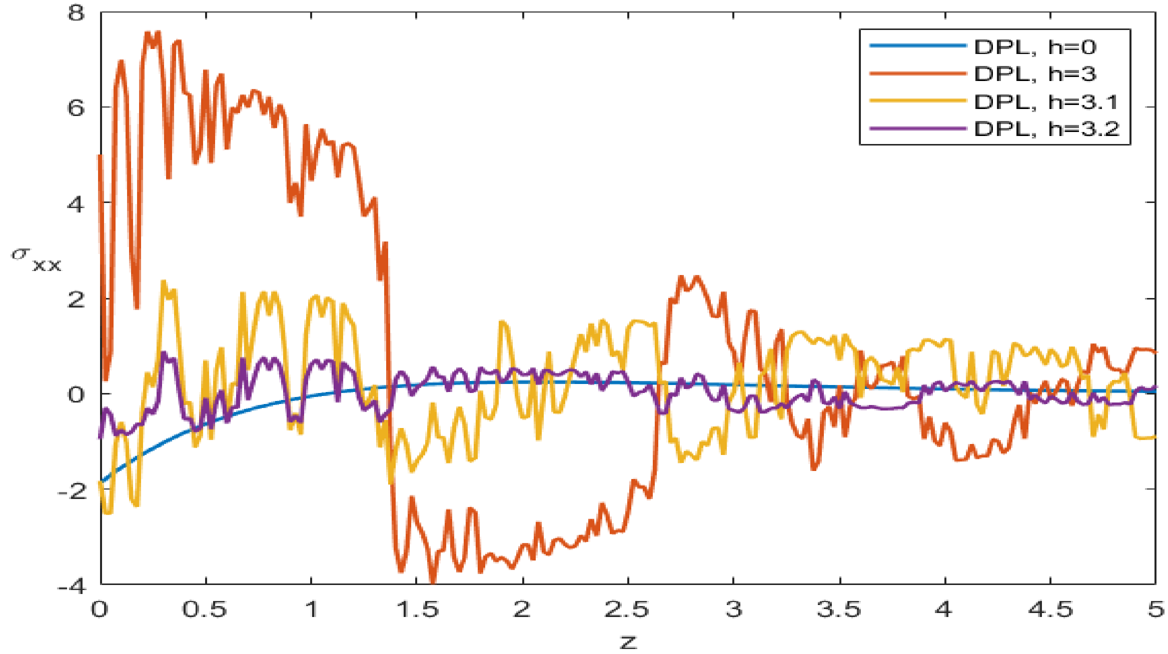

Figure 12. The stress tensor (σ_{xx}) distributions for the DPL model

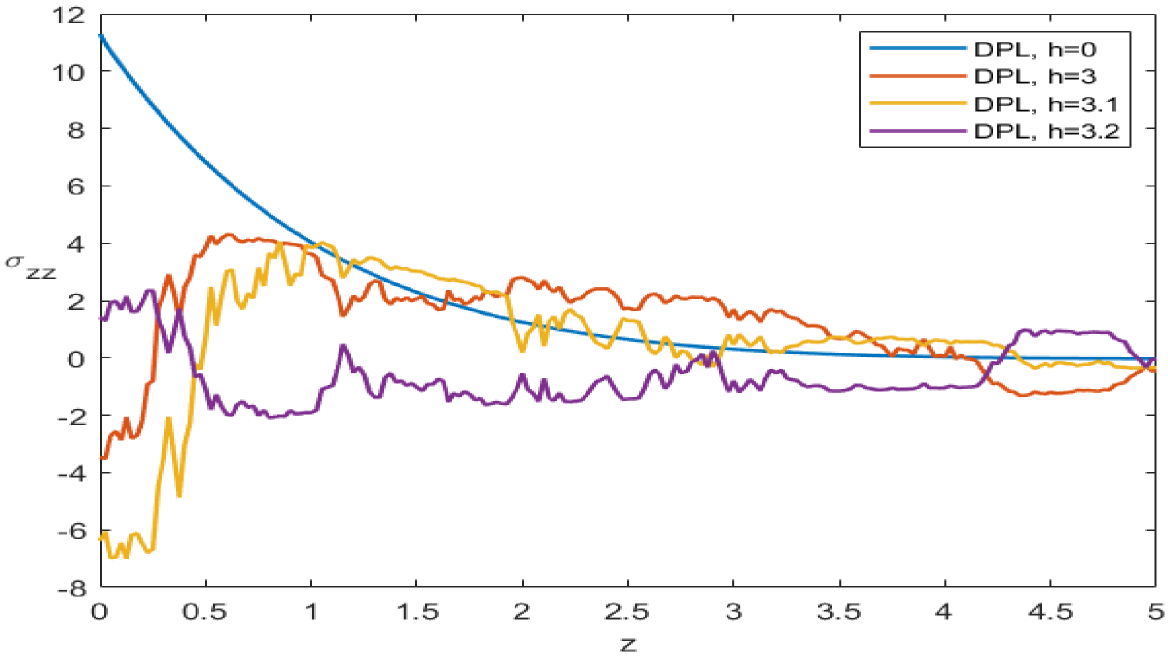

Figure 13. The stress tensor (σ_{zz}) distributions for the DPL model

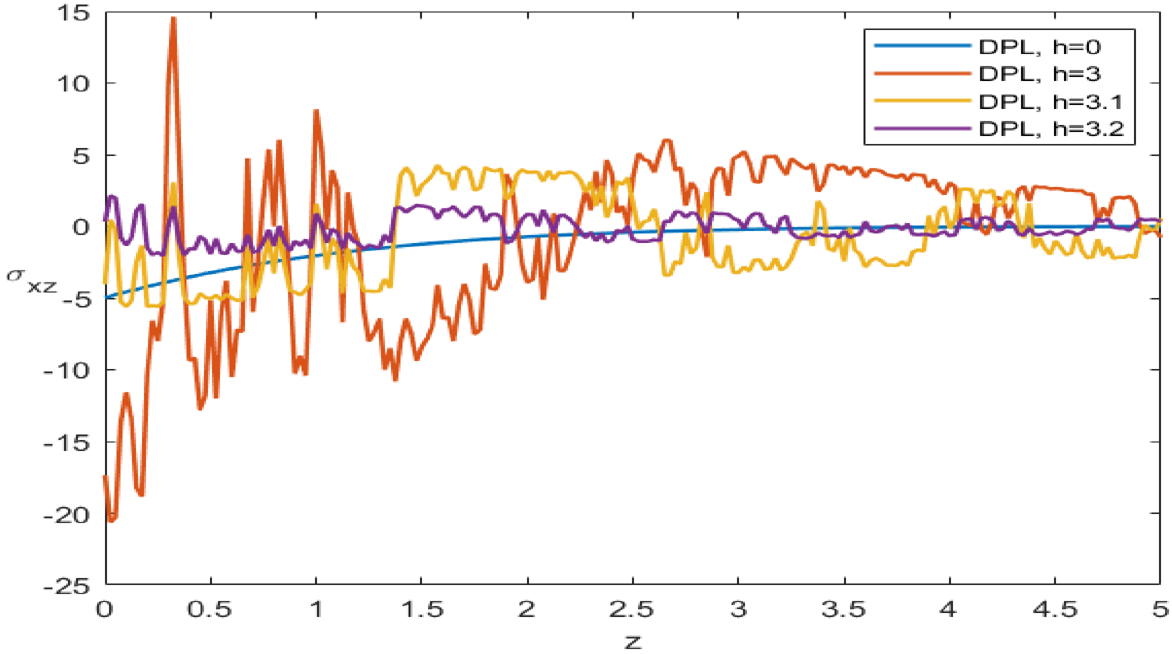

Figure 14. The stress tensor (σ_{xz}) distributions for the DPL model

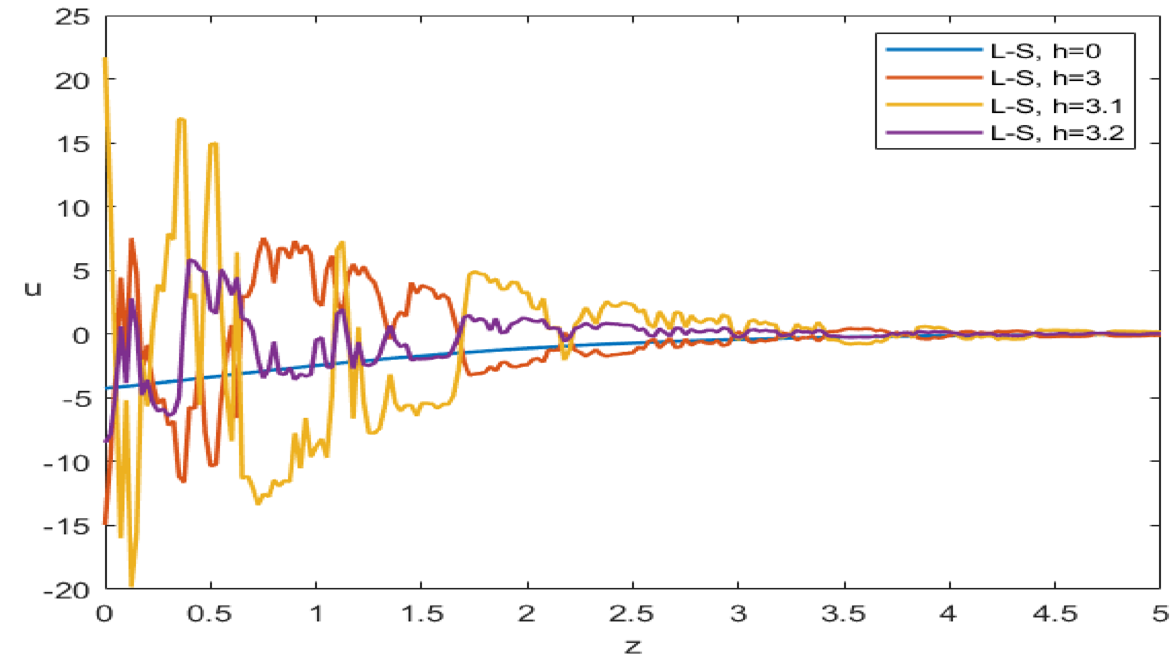

Figure 15. The horizontal displacement distributions for the L-S theory

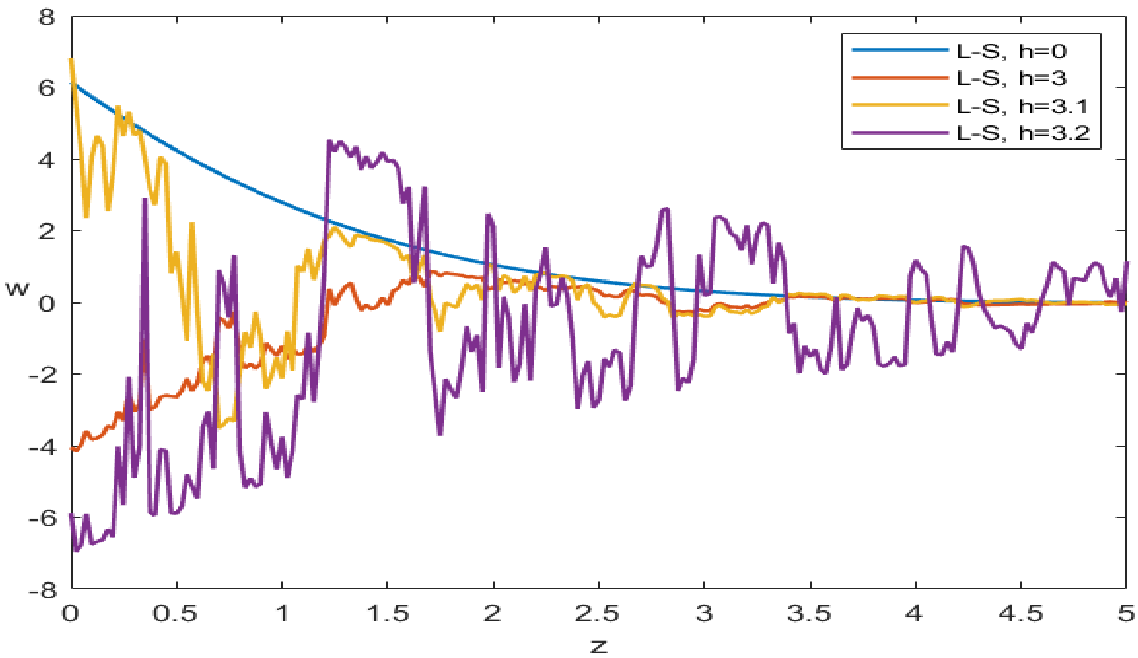

Figure 16. The vertical displacement distributions for the L-S theory

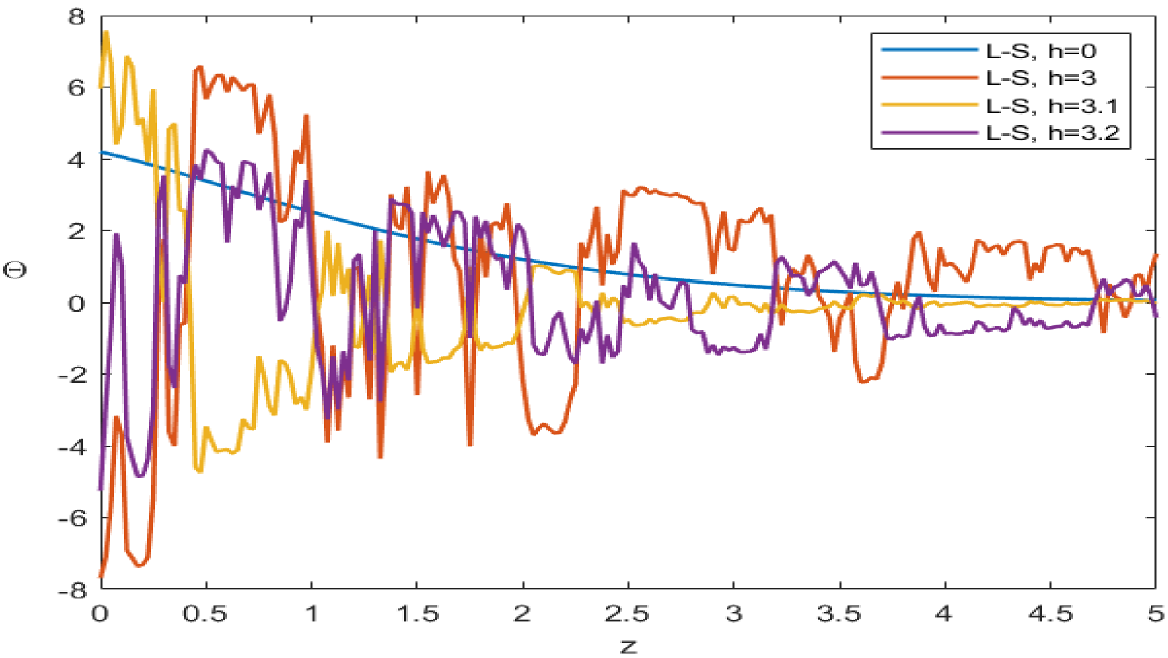

Figure 17. The temperature distributions for the L-S theory

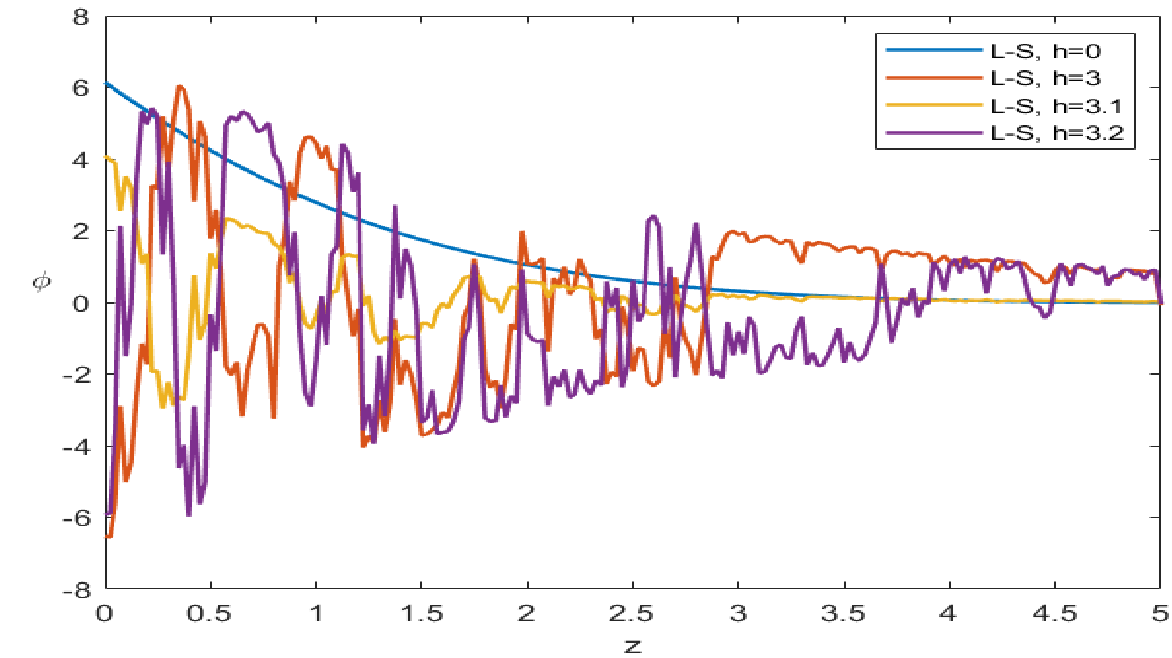

Figure 18. The micro-elongated distributions for the L-S theory

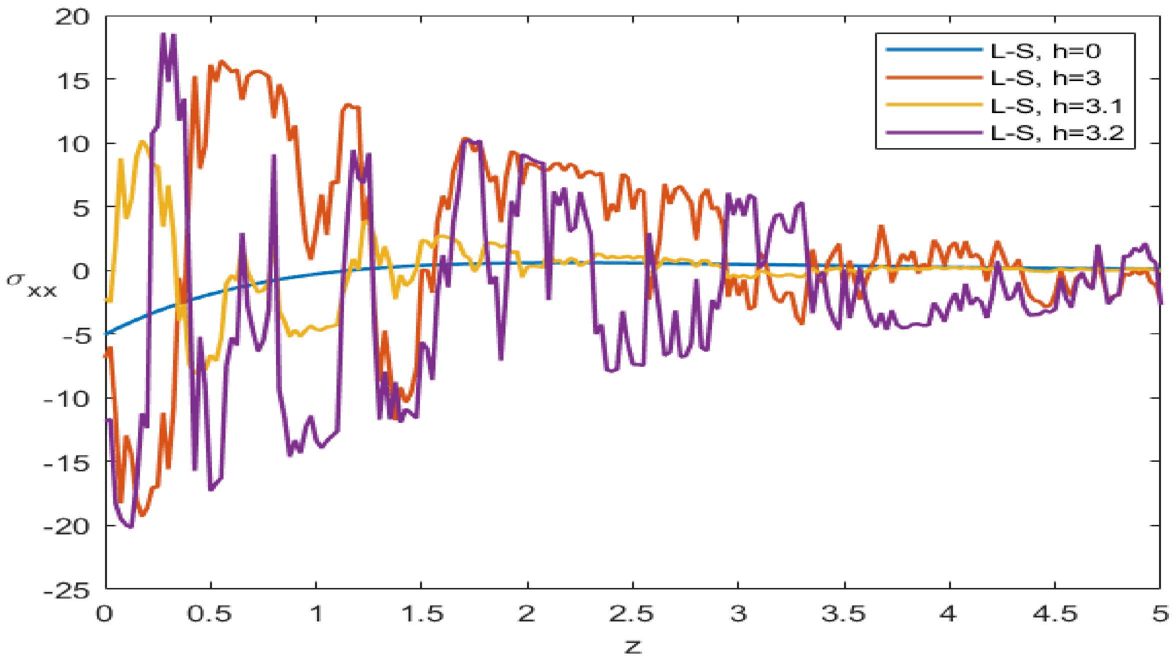

Figure 19. The stress tensor (σ_{xx}) distributions for the L-S theory

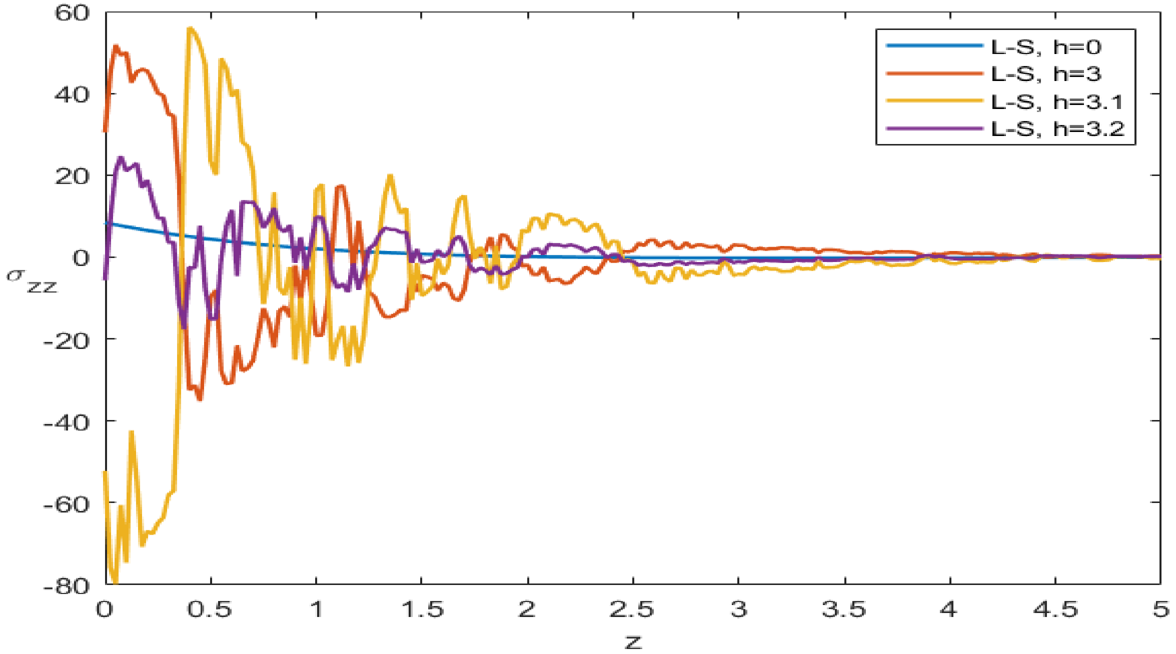

Figure 20. The stress tensor (σ_{zz}) distributions for the L-S theory

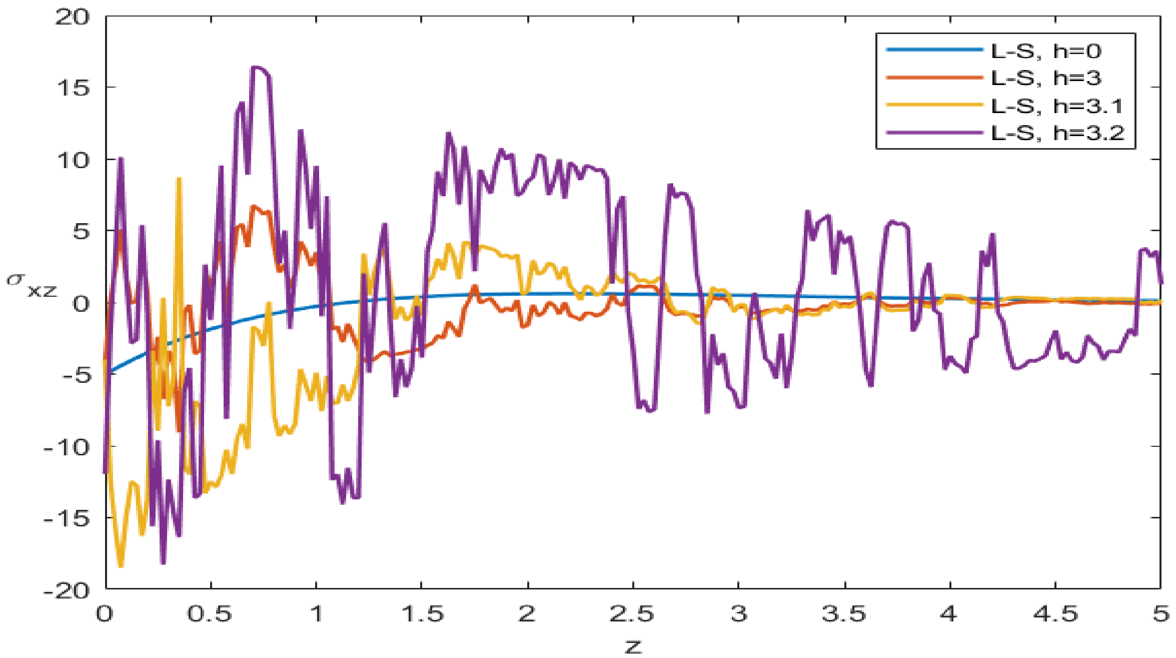

Figure 21. The stress tensor (σ_{xz}) distributions for the L-S theory

5. Conclusion

In this paper, a comprehensive analytical and numerical investigation has been carried out to examine how rotation and stochastic disturbances effect wave propagation in a micro-elongated thermo-elastic half-space within the frameworks of the L-S theory, DPL model, and RDPL model. The governing equations describing mechanical displacement, temperature, micro-elongation, and stress components were formulated to incorporate the combined effects of finite thermal wave speed, micro-elongation, phase-lag behavior, rotational inertia, and stochastic excitation. By combining non-dimensionalization and the stochastic transform, the original stochastic partial differential equations system was reduced to stochastic ordinary differential equations, which were solvable and allowed for explicit assessment of the dynamic fields.

The analytical solutions, together with the extensive set of numerical plots, illustrated several significant physical insights. The presence of rotation introduces noticeable modifications to all thermo-mechanical responses through centrifugal and Coriolis effects, resulting in altered amplitudes, modified wave speeds, and directional sensitivities that are absent in non-rotating media. The comparison of deterministic and stochastic responses revealed that stochastic excitation consistently increases oscillatory behavior, particularly in micro-elongation and stress components. The introduction of stochastic leads to fluctuating waveforms and enhanced irregularity, emphasizing the sensitivity of micro-elongated media to random thermal disturbances. Among the three theories, the RDPL model showed the most stable and physically realistic response under random perturbations due to its higher-order phase-lag refinements, whereas the L-S theory displayed the largest deviations under noise.

List of Nomenclature

Quantity	Definition
$\mathbf{u}$	Displacement vector,
α_t	Coefficient of linear thermal expansion, where $\gamma = (3\lambda + 3\mu)\,\alpha_t$,
λ and μ	Constants of Lame,
j^*	Microinertia,
T_0	Reference temperature,
Ω	Rotation,
λ_0, λ_1, a_0	Constants of micro-elongational,
φ	Micro-elongational scalar,
Θ	Temperature,
c_e	Specific heat,
ρ	Density,
t	Time,
k	Thermal conductivity,
τ_θ	Phase-lag of the temperature gradient,
σ_{ij}	Component of stress tensor,
τ_q	Phase-lag of the heat flux.

Conflict of Interest

The authors declare there is no existing conflict of interest.

References

1.Zenkour, A. M. (2020). Thermo-diffusion of solid cylinders based upon refined dual-phase-lag models. *Multidiscipline Modeling in Materials and Structures*, 16(6), 1417-1434.

2.Khamis, A. K., El-Bary, A. A., Lotfy, K., and Bakali, A. (2020). Photothermal excitation processes with refined multi dual phase-lags theory for semiconductor elastic medium. *Alexandria Engineering Journal*, 59(1), 1-9.

3.Abouelregal, A. E. (2021). Modified fractional thermoelasticity model with multi-relaxation times of higher order: application to spherical cavity exposed to a harmonic varying heat. *Waves in Random and Complex Media*, 31(5), 812-832.

4.Kutbi, M. A. and Zenkour, A. M. (2022). Refined dual-phase-lag Green–Naghdi models for thermoelastic diffusion in an infinite medium. *Waves in Random and Complex Media*, 32(2), 947-967.

5.Jeyaraman, P., Mahesh, S., Selvamani, R., Dimitri, R., and Tornabene, F. (2022). Multi thermal waves in a thermo diffusive piezo electric functionally graded rod via refined multi-dual phase-lag model. *Curved and Layered Structures*, 9(1), 105-115.

6.Zenkour, A. M., Saeed, T., and Aati, A. M. (2023). Refined dual-phase-lag theory for the 1D behavior of skin tissue under ramp-type heating. *Materials*, 16(6), 2421.

7.Bhattacharya, D., and Kanoria, M. (2024). Refined four-phase lag model for elasto-thermodiffusive interaction with harmonically varying heat sources. *Mechanics of Time-Dependent Materials*, 28(3), 1853-1872.

8.Hafed, Z. S., Abo-Dahab, S. M., Kilany, A. A., and Ahmed, S. E. (2025). Electromagnetic field on a photothermal semiconducting voids medium under Lord–Shulman and refined multi-phase lag models in thermoelasticity. *International Journal of Modern Physics B*, 39(01), 2550007.

9.Ailawalia, P., Sachdeva, S. K., and Pathania, D. S. (2015). Plane strain deformation in a thermoelastic microelongated solid with internal heat source. *International Journal of Applied Mechanics and Engineering,* 20(4).

10.Lotfy, K. (2022). Thermo-mechanical waves of excited microelongated semiconductor layer during photothermal transport processes. *Waves in Random and Complex Media*, 1-17.

11.Hilal, M. I. (2022). Thermomechanical interactions of rotating thermoelastic magneto-microelongated medium heated by laser and initially stressed via non-local elasticity and GN III. *Acta Mechanica*, 233(12), 5183-5197.

12.El-Sapa, S., Alhejaili, W., Lotfy, K., and El-Bary, A. A. (2023). Response of excited microelongated nonlocal semiconductor layer thermomechanical waves to photothermal transport processes. *Acta Mechanica*, 234(6), 2373-2388.

13.Yadav, K., Sheoran, D., and Kalkal, K. K. (2025). Reflection of plane waves in a microelongated thermoelastic porous medium with Hall current under modified Green–Lindsay model. *Acta Mechanica*, 236(2), 1359-1380.

14.Kadian, P., Kumar, S., Hooda, N., and Sangwan, M. (2024). Reflection of plane waves in a non-local viscothermoelastic half-space under variable thermal conductivity and microelongation effects. *Journal of Thermal Stresses*, 47(11), 1479-1499.

15.Kadian, P., Kumar, S., and Sangwan, M. (2024). Effect of inclined mechanical load on a rotating microelongated two temperature thermoelastic half space with temperature dependent properties. *Journal of Vibration Engineering & Technologies*, 12(3), 4053-4074.

16.Alshehri, A. M., Lotfy, K., and Ibrahim, E. (2024). A novel model of microelongation thermomechanical photoacoustic waves in excited semiconductor materials. *Results in Physics*, 63, 107881.

17.Abd-Alla, A. M., Abo-Dahab, S. M., and Alsharif, A. (2024). Thermal shock behaviour on generalized thermoelastic medium under initial stress with rotation. *Mechanics of Solids*, 59(5), 2861-2875.

18.Makkad, G., Khalsa, L., Abouelregal, A., and Varghese, V. (2025). Analysis of magneto-thermoviscoelastic behavior in rotating thermal-infused nanorods: exploring thermomass dynamics and Klein–Gordon nonlocality effects. *Acta Mechanica*, 1-25.

19.Abo-Dahab, S. M., Jaradat, E. K., Gafel, H. S., and Elidy, E. S. (2025). Rotational Influence on Wave Propagation in Semiconductor Nanostructure Thermoelastic Solid with Ramp-Type Heat Source and Two-Temperature Theory. *Axioms*, 14(8), 560.

20.Alsaeed, S. S. and Abouelregal, A. E. (2025). Advanced thermoelastic analysis of rotating nanobeams with temperature-dependent properties: incorporating non-local effects, size dependence, and thermal conduction models. *Mechanics Based Design of Structures and Machines*, 1-29.

21.Salah, D. M., Abd-Alla, A. M., and El-Kabeir, S. M. M. (2025). Magneto-Thermoelastic Response of a Rotating Medium with Double Porosity under Initial Stress. *Mechanics of Solids*, 1-19.

22.Wang, H., He, T., and Ma, Y. (2025). Investigation on the electro-magneto-thermoviscoelastic response of multilayer rotating hollow cylinder based on two-temperature theory and fractional-order viscoelastic systems. *Mechanics of Advanced Materials and Structures*, 32(17), 4196-4224.

23.Lotfy, K., El-Bary, A., and Elidy, E. (2024). Magneto-photo-thermoelastic excitation rotating semiconductor medium based on moisture diffusivity. *Computer Modeling in Engineering & Sciences*, 141(1), 107.

24.Chiba, R. and Sugano, Y. (2007). Stochastic thermoelastic problem of a functionally graded plate under random temperature load. *Archive of Applied Mechanics*, 77(4), 215-227.

25.Chiba, R. and Sugano, Y. (2008). Stochastic analysis of a thermoelastic problem in functionally graded plates with uncertain material properties. *Archive of Applied Mechanics*, 78(10), 749-764.

26.Sherief, H. H., El-Maghraby, N. M., and Allam, A. A. (2017). Stochastic thermal shock problem and study of wave propagation in the theory of generalized thermoelastic diffusion. *Mathematics and Mechanics of Solids*, 22(9), 1767-1789.

27.Lotfy, K., Ahmed A., El-Bary, A., El-Shekhipy, A., and Tantawi, R. S. (2022). A novel stochastic photo-thermoelasticity model according to a diffusion interaction processes of excited semiconductor medium. *The European Physical Journal Plus*, 137(8), 972.

28.Lotfy, K., Ahmed, A., El-Bary, A. A., Tantawi, R. S., Elidy, E. S., Saeed, A. M., and Mahdy, A. M. S. (2024). A Stochastic photoacoustic study influenced by white noise on thermoelastic waves in semiconductor medium. *Semiconductors*, 58(12), 948-959.

29.Rezk, E. G., Ismail, G. M., Ahmed, A., Lotfy, K., El-Bary, A. A., Can, E., and Elidy, E. S. (2025). A stochastic dual-phase-lag two-temperature photo-thermoelastic model for double-porosity semiconductors with initial stress. *Scientific Reports*.

30. Mohammed, W. W., Cesarano, C., Alqsair, N. I., and Sidaoui, R. (2024). The impact of Brownian motion on the optical solutions of the stochastic ultra-short pulses mathematical model. *Alexandria Engineering Journal*, 101, 186-192.

31. Ashraf, R., Amanat, F., Ashraf, F., Owyed, S., Matoog, R. T., Mahmoud, M., and Akgül, A. (2024). Soliton solutions for the (4+ 1)-dimensional Fokas equation using integration techniques. *Alexandria Engineering Journal*, 107, 61-72.